GEORGE S. DULIKRAVICH
FED-Vol. 66

ADVANCES AND APPLICATIONS IN COMPUTATIONAL FLUID DYNAMICS

presented at

THE WINTER ANNUAL MEETING OF
THE AMERICAN SOCIETY OF MECHANICAL ENGINEERS
CHICAGO, ILLINOIS
NOVEMBER 27–DECEMBER 2, 1988

sponsored by

THE FLUIDS ENGINEERING DIVISION, ASME

edited by

O. BAYSAL
OLD DOMINION UNIVERSITY

THE AMERICAN SOCIETY OF MECHANICAL ENGINEERS
United Engineering Center 345 East 47th Street New York, N.Y. 10017

ITERATIVE ACCELERATION AND PHYSICALLY BASED DISSIPATION FOR EULER EQUATIONS OF GASDYNAMICS

G. S. Dulikravich, Associate Professor
D. J. Dorney and S. Lee, Graduate Students
Department of Aerospace Engineering
The Pennsylvania State University
University Park, Pennsylvania

ABSTRACT

A new algorithm for the acceleration of explicit iterative schemes for a system of partial differential equations has been developed. The method is based on the idea of allowing each partial differential equation in the system to approach the converged solution at its own optimal speed. The DMR (Distributed Minimal Residual) method allows a separate sequence of optimal weighting factors to be used for each component of the general solution vector. The acceleration scheme was applied to the system of time-dependent Euler equations of inviscid gasdynamics in conjunction with the finite volume Runge-Kutta explicit time-stepping method with the Jameson's Artificial Dissipation (AD) terms and the newly formulated Physically Based Dissipation (PBD) model. The PBD model uses physical dissipation terms from the Navier-Stokes equations of gasdynamics, while enforcing slip boundary conditions of inviscid gasdynamics and utilizing spatially varying viscosity coefficients. Tests were performed for various flow conditions, including internal flow, flow around a cylinder and flow over an airfoil with AD and PBD. Using DMR, between 30% and 70% of the computational efforts were saved in the subsonic compressible flow calculations.

INTRODUCTION

When the Euler equations of inviscid gasdynamics are solved using a central difference scheme (e.g., a Runge-Kutta time-stepping scheme [1]), decoupling of odd and even grid points allows oscillations to develop which cause instabilities in the numerical algorithm. These oscillations can be damped by either explicitly or implicitly adding a certain amount of artificial dissipation [2].

Contemporary artificial dissipation models for central difference schemes usually consist of an ad hoc combination of second order and fourth order artificial (non-physical) dissipation terms [2]. The second order terms are used to damp oscillations in shock regions, while the fourth order terms ensure monotonic convergence to steady state in smooth flow regions [1,3,4].

Most of the existing artificial dissipation formulations are intuitive [5,1]. The intuitive formulations generate artificial dispersion terms [4], which are partially neutralized by adding higher order artificial dissipation terms. Only after a trial-and-error process can it be found that the coefficients multiplying second and fourth order artificial dissipation which are appropriate for very low speeds are orders of magnitude smaller then the coefficients that are appropriate for transonic speeds. It has been shown that using different amounts of second order and fourth order dissipation can produce different numerical results that are often misleading, especially in the case of transonic shocked flows with separation [6,7].

It can be concluded that the intuitive formulations for artificial dissipation which have been favored in the past are only marginally reliable. Their accuracy is still an open question [6,7,8,9,10] since there is no known exact solution to the Euler equations for a shocked flow with inviscid separation. Thus, the existing artificial dissipation models are subject to constant modifications [4,11,12,13] in order to meet the requirements posed by different flow speed regimes.

One objective of this paper is to introduce a physically consistent [14] model for the dissipation to be used in the numerical solution of Euler and Navier-Stokes equations. The other objective is to introduce a new concept for convergence acceleration.

Several attempts have been made in the past to accelerate the iterative convergence of the Runge-Kutta method [15]. They include local time stepping [1], implicit residual smoothing [1], enthalpy damping [1] and multigrid techniques [12,16]. Also, the extrapolation procedure based on the power method and the Minimal Residual Method (MRM) were applied [16] to the Runge-Kutta method. In the MRM [16], a weighted combination of the corrections at consecutive iteration levels are extrapolated and the weights are chosen to minimize the L_2 norm of the future residual. Since the extrapolation was performed without considering the properties of the governing equations, it may upset the solution procedure. The GNLMR (Generalized Non-Linear Minimal

Residual) method [17,18,19,20] used the information from the governing equations. It has been applied successfully to a number of single nonlinear partial differential equations including the Euler equations.

Both MRM and GNLMR method use the same sequence of optimal weights for the corrections to every equation in a system. Since each component of the solution vector has its own convergence speed, the sequence of optimal weights should be allowed to vary from component to component. Thus, the objective of this paper is to present the theory constituting the Distributed Minimal Residual DMR method and todemonstrate the advantages of the new algorithm with a number of computational examples.

EULER EQUATIONS OF GASDYNAMICS

The two-dimensional Euler equations in conservative form and cartesian coordinates can be written as

$$\bar{Q}_t + \bar{E}_x + \bar{F}_y = 0 \tag{1}$$

Here, the subscripts t, x, y represent partial derivatives with respect to time, and to x, y coordinates, respectively. The general vectors

$\bar{Q}$, $\bar{E}$, and $\bar{F}$ are defined as

$$\bar{Q} = \begin{bmatrix} \rho \\ \rho u \\ \rho v \\ \rho e_o \end{bmatrix} \qquad \bar{E} = \begin{bmatrix} \rho u \\ \rho u^2+p \\ \rho uv \\ \rho u h_o \end{bmatrix} \qquad \bar{F} = \begin{bmatrix} \rho v \\ \rho vu \\ \rho v^2+p \\ \rho v h_o \end{bmatrix} \tag{2}$$

where ρ, p, u, v, e_o and h_o are the non-dimensional values of local density, thermodynamic pressure, x-component of velocity, y-component of velocity, total mass-specific energy and total mass-specific enthalpy, respectively.

Equation of state for a calorically perfect gas can be expressed as

$$p = (\gamma-1)\left(\rho e_o - \frac{1}{2}\left(\frac{(\rho u)^2}{\rho} + \frac{(\rho v)^2}{\rho}\right)\right) \tag{3}$$

where γ represents the ratio of specific heats. The total mass-specific enthalpy, h_o, is defined as

$$h_o = e_o + \frac{p}{\rho} \tag{4}$$

For the analysis of flows about arbitrary geometries, the formulation can be generalized by using, say, fixed body-fitted non-orthogonal coordinates ξ and η, so that

$$\xi = \xi(x,y) \; ; \; \eta = \eta(x,y) \tag{5}$$

Thus, in the computational (ξ,η) domain, the two-dimensional Euler equations in a strongly conservative form become

$$Q_t + E_\xi + F_\eta = 0 \tag{6}$$

where

$$Q = \frac{1}{D}\begin{bmatrix} \rho \\ \rho u \\ \rho v \\ \rho e_o \end{bmatrix} \quad E = \frac{1}{D}\begin{bmatrix} \rho U \\ \rho uU + p\xi_x \\ \rho vU + p\xi_y \\ \rho h_o U \end{bmatrix} \quad F = \frac{1}{D}\begin{bmatrix} \rho V \\ \rho uV + p\eta_x \\ \rho vV + p\eta_y \\ \rho h_o V \end{bmatrix} \tag{7}$$

Here

$$D = \det\left(\frac{\partial(\xi,\eta)}{\partial(x,y)}\right) = \frac{1}{\det\left(\frac{\partial(x,y)}{\partial(\xi,\eta)}\right)} = 1/\begin{vmatrix} x_\xi & x_\eta \\ y_\xi & y_\eta \end{vmatrix} \tag{8}$$

Thus

$$\xi_x/D = y_\eta; \quad \eta_x/D = -y_\xi \; ; \; \xi_y/D = -x_\eta; \; \eta_y/D = x_\xi \tag{9}$$

The contravariant components U,V of the velocity vector are related to the cartesian components u,v as follows

$$\begin{bmatrix} U \\ V \end{bmatrix} = \begin{bmatrix} \xi_x & \xi_y \\ \eta_x & \eta_y \end{bmatrix} \begin{bmatrix} u \\ v \end{bmatrix} \tag{10}$$

EXISTING ARTIFICIAL DISSIPATION MODEL

A typical stage of the multistage Runge-Kutta [15] time-stepping scheme for the Euler equations [1,4] is

$$Q^{(n)} = Q^{(o)} + \alpha_n \Delta t \, (E_\xi^{(n-1)} + F_\eta^{(n-1)} + P) \tag{11}$$

where $P_{i,j}$ is the artificial dissipation [1,4] given as

$$P_{i,j} = (P^\xi_{i+1/2,j} - P^\xi_{i-1/2,j}) + (P^\eta_{i,j+1/2} - P^\eta_{i,j-1/2}) \tag{12}$$

Calculation of the artificially dissipative terms is done similarly [1,4] for all conservation laws. For example,

$$P^\xi_{i+\delta/2,j} = \varepsilon^{(2)}_{i+\delta/2,j} \, Q^\xi_{i+\delta/2,j} - \varepsilon^{(4)}_{i+\delta/2,j}\left(\theta_{i+\delta,j} \, Q^{\xi\xi}_{i+\delta,j} - \theta_{i,j} \, Q^{\xi\xi}_{i,j}\right) \tag{13}$$

$$P^\eta_{i,j+\delta/2} = \varepsilon^{(2)}_{i,j+\delta/2} \, Q^\eta_{i,j+\delta/2} - \varepsilon^{(4)}_{i,j+\delta/2}\left(\theta_{i,j+\delta} \, Q^{\eta\eta}_{i,j+\delta} - \theta_{i,j} \, Q^{\eta\eta}_{i,j}\right) \tag{14}$$

where $\delta = \pm 1$. The remaining terms are defined as follows:

$$\theta_{i,j} = \frac{1}{(D\,\Delta t^*)_{i,j}} \tag{15}$$

$$Q^\xi_{i+\delta/2,j} = Q_{i+\delta,j} - Q_{i,j} \tag{16}$$

$$Q^{\xi\xi}_{i+\delta,j} = Q_{i+2\delta,j} - 2Q_{i+\delta,j} + Q_{i,j} \tag{17}$$

$$Q^{\xi\xi}_{i,j} = Q_{i+1,j} - 2Q_{i,j} + Q_{i-1,j} \tag{18}$$

with similar expressions for the other terms of this type. The coefficients of second and fourth order artificial dissipation are defined [4,1], respectively, as

$$\epsilon^{(2)}_{i+\delta/2,j} = \theta_{i,j}\ \kappa^{(2)}\ \max\left(\nu^{\xi\xi}_{i,j}\ ;\ \nu^{\xi\xi}_{i+\delta,j}\right) \tag{19}$$

$$\epsilon^{(4)}_{i+\delta/2,j} = \max\left(0;\ \kappa^{(4)} - \kappa^{(2)}\max\left(\nu^{\xi\xi}_{i,j}\ ;\ \nu^{\xi\xi}_{i+\delta,j}\right)\right) \tag{20}$$

with similar expressions for the other terms of this type, where $\kappa^{(2)} = 1/4$ to $1/2$ and $\kappa^{(4)} = 1/128$ to $1/64$ are typical constants [3]. Here, the local "directional pressure sensor" is defined as

$$\nu^{\xi\xi}_{i,j} = \left|\frac{p_{i+1,j} - 2p_{i,j} + p_{i-1,j}}{p_{i+1,j} + 2p_{i,j} + p_{i-1,j}}\right| \tag{21}$$

Similarly

$$\nu^{\eta\eta}_{i,j} = \left|\frac{p_{i,j+1} - 2p_{i,j} + p_{i,j-1}}{p_{i,j+1} + 2p_{i,j} + p_{i,j-1}}\right| \tag{22}$$

PHYSICALLY BASED DISSIPATION (PBD) MODEL

Instead of using an intuitive non-physical formulation for the artificial dissipation, we suggest that the dissipation should be based on actual physical dissipation, that is, it should be physically consistent. We propose that to solve the Euler equations of inviscid flow, one should actually solve the complete Navier-Stokes equations of viscous and heat conducting flow subject to perfect slip boundary conditions and spatially varying coefficients of viscosity [14]. Thus, the PBD model represents a physically consistent formulation since the Euler equations of inviscid gasdynamics represent an extreme case of Navier-Stokes equations when the physical dissipation becomes negligible.

The Navier-Stokes equations of unsteady, viscous, laminar flow allowing for heat conduction (assuming Fourier's law) expressed in non-dimensional form and non-orthogonal curvilinear coordinates can be summarized as

$$Q_t + E_\xi + F_\eta = \frac{1}{Re}\left(E^v_\xi + F^v_\eta\right) \tag{23}$$

where R_e is the Reynolds number and E^v_ξ, F^v_η incorporate physically dissipative terms due to shear viscosity, secondary viscosity and heat conductivity. The generalized viscous flux vectors are

$$E^v = \frac{1}{D}\begin{bmatrix} 0 \\ E_1 \\ E_2 \\ E_3 \end{bmatrix}\ ;\quad F^v = \frac{1}{D}\begin{bmatrix} 0 \\ F_1 \\ F_2 \\ F_3 \end{bmatrix} \tag{24}$$

where

$$\begin{bmatrix} E_1 & E_2 \\ F_1 & F_2 \end{bmatrix} = \begin{bmatrix} \xi_x & \xi_y \\ \eta_x & \eta_y \end{bmatrix}\begin{bmatrix} \tau_{xx} & \tau_{xy} \\ \tau_{yx} & \tau_{yy} \end{bmatrix} \tag{25}$$

and

$$\begin{bmatrix} E_3 \\ F_3 \end{bmatrix} = \begin{bmatrix} \xi_x & \xi_y \\ \eta_x & \eta_y \end{bmatrix}\begin{bmatrix} \tau_{xx} & \tau_{xy} \\ \tau_{yx} & \tau_{yy} \end{bmatrix}\begin{bmatrix} u \\ v \end{bmatrix} - \begin{bmatrix} \xi_x & \xi_y \\ \eta_x & \eta_y \end{bmatrix}\begin{bmatrix} q_x \\ q_y \end{bmatrix} \tag{26}$$

Here, the components of the non-dimensional viscous stress tensor expressed in terms of ξ,η coordinates are:

$$\tau_{xx} = \mu''\left(\xi_x u_\xi + \eta_x u_\eta\right) + \lambda\left(\xi_y v_\xi + \eta_y v_\eta\right) \tag{27}$$

$$\tau_{xy} = \mu''\left(\xi_y u_\xi + \eta_y u_\eta + \xi_x v_\xi + \eta_x v_\eta\right) \tag{28}$$

and the non-dimensional heat conduction flux is

$$q_x = \frac{\mu}{(\gamma-1)M_\infty^2 Pr}\left(\xi_x T_\xi + \eta_x T_\eta\right) \tag{29}$$

Here, $\mu'' = 2\mu + \lambda$ is the longitudinal viscosity coefficient, M_∞ is the Mach number of the uniform flow at infinity, Pr is the Prandtl number and T is the absolute temperature. Since Rankine-Hugoniot shock jump conditions are possible only [21] if Stokes hypothesis ($\lambda/\mu = -2/3$) is enforced, we use this relation in actual computations.

In the PBD formulation, the shear viscosity coefficient, μ, is forced to vary throughout the flowfield by means of an appropriate "sensor". The physical thermodynamic pressure, p, appears in the equations of gasdynamics in the form of its first derivative. Consequently, we have decided to use the pressure sensor which is based on the streamwise first derivative of the pressure, that is,

$$\mu_{i,j} = \frac{C\mu}{\left(u^2 + v^2\right)^{1/2}}\left(Up_\xi + Vp_\eta\right) = C\ p_s\mu \tag{30}$$

Here, C is a user specified constant. Using numerical experimentation, we have found that $10 < C < 20$ for the range of freestream Mach numbers $0.1 < M_\infty < 30$. We have experimented with a number of different "sensors" and found that the three-point average streamwise first derivative of pressure gives a robust scheme

$$\mu_{i,j} = \left(\mu_{i+1,j} + \mu_{i,j} + \mu_{i-1,j}\right)/3 \tag{31}$$

Obviously, this is just one among many possible suggestions for the "sensor." Other choices might be, for example,

sensor based on divergence:

$$\mu_{i,j} = C\,|\nabla\cdot\vec{V}|\,\mu \tag{32}$$

sensor based on Mach number:

$$\mu_{i,j} = \mu C\left(M_\xi U + M_\eta V\right)/|\vec{V}| \tag{33}$$

sensor based on M^2:

$$\mu_{i,j} = \mu C(M_\xi^2 U + M_\eta^2 V)/|\vec{V}| \tag{34}$$

DISTRIBUTED MINIMAL RESIDUAL (DMR) METHOD

Global residual of the finite volume method at time level t can be expressed in two dimensions as

$$r^t = \iint \frac{\partial Q}{\partial t}\, dS = -\iint \left(\frac{\partial E}{\partial \xi} + \frac{\partial F}{\partial \eta}\right) dS \tag{35}$$

where S is the surface area of the single grid cell and components Q, E and F of the generalized solution vector are defined in Eq. 2. In the case of, say, four-step explicit Runge-Kutta algorithm one needs four intermediate time steps to advance the solution from the global time level (t) to (t+1).

We plan to use corrections from M previous consecutive time levels to update the value of Q to (t+1) global time level. Thus,

$$Q^{t+1} = Q^t + \sum_m^M \Omega^m \tag{36}$$

where

$$\Omega^m = \begin{bmatrix} \omega_1^m \Delta_1^m \\ \omega_2^m \Delta_2^m \\ \vdots \\ \omega_L^M \Delta_L^M \end{bmatrix} \tag{37}$$

and Δ_ℓ^m are the corrections for each of the $\ell = 1,\ldots,L$ equations in the system (Eq. 2) at each of the $m=1,\ldots, M$ global time steps. Therefore, substituting Eq. 36 in Eq. 35, the new local residual for the single cell will be

$$r^{t+1} = -\iint \left[\frac{\partial}{\partial \xi} E\,(Q^t + \sum_m^M \Omega^m) + \frac{\partial}{\partial \eta} F\,(Q^t + \sum_m^M \Omega^m)\right] dS \tag{38}$$

Using a Taylor series expansion truncated after the first term results in

$$r^{t+1} = r^t - \sum_m^M \iint \left[\frac{\partial}{\partial \xi}\left(\frac{\partial E}{\partial Q}\Omega^m\right) + \frac{\partial}{\partial \eta}\left(\frac{\partial F}{\partial Q}\Omega^m\right)\right] dS \tag{39}$$

Define the global residual R^t as a sum of the squares of the local residuals, that is,

$$R^t = \sum_i^I \sum_j^J (r^t)^* (r^t) \tag{40}$$

where I and J define the grid size and the superscript * designates the transpose. Then, the global residual at the next global time level will be

$$R^{t+1} = \sum_i^I \sum_j^J \left\{r^t - \sum_n^M \iint \left[\frac{\partial}{\partial \xi}\left(\frac{\partial E}{\partial Q}\Omega^n\right) + \frac{\partial}{\partial \eta}\left(\frac{\partial F}{\partial Q}\Omega^n\right)\right] dS\right\}^* \cdot \left\{r^t - \sum_m^M \iint \left[\frac{\partial}{\partial \xi}\left(\frac{\partial E}{\partial Q}\Omega^m\right) + \frac{\partial}{\partial \eta}\left(\frac{\partial F}{\partial Q}\Omega^m\right)\right] dS\right\} \tag{41}$$

To minimize R^{t+1}, it is necessary to use the values of ω_ℓ that satisfy

$$\frac{\partial R^{t+1}}{\partial \omega_\ell^m} = 0 \tag{42}$$

for all m and ℓ. Thus, from Eq. 41 and Eq. 42 it follows that

$$\sum_i^I \sum_j^J (r^t)^* \left\{\iint \left[\frac{\partial}{\partial \xi}\left(\frac{\partial E}{\partial Q}\frac{\partial \Omega^m}{\partial \omega_\ell^m}\right) + \frac{\partial}{\partial \eta}\left(\frac{\partial F}{\partial Q}\frac{\partial \Omega^m}{\partial \omega_\ell^m}\right)\right] dS\right\}$$

$$= \sum_i^I \sum_j^J \sum_n^M \left\{\iint \left[\frac{\partial}{\partial \xi}\left(\frac{\partial E}{\partial Q}\Omega^n\right) + \frac{\partial}{\partial \eta}\left(\frac{\partial F}{\partial Q}\Omega^n\right)\right] dS\right\}^* \cdot \left\{\iint \left[\frac{\partial}{\partial \xi}\left(\frac{\partial E}{\partial Q}\frac{\partial \Omega^m}{\partial \omega_\ell^m}\right) + \frac{\partial}{\partial \eta}\left(\frac{\partial F}{\partial Q}\frac{\partial \Omega^m}{\partial \omega_\ell^m}\right)\right] dS\right\} \tag{43}$$

where $\frac{\partial \Omega^m}{\partial \omega_\ell^m} = (\Delta_k^m \delta_{k\ell})$ and $\delta_{k\ell}$ is the Kronecker delta.

Notice that

$$\frac{\partial E}{\partial Q}\Omega^n = \sum_q^L \omega_q^n \frac{\partial E}{\partial Q}\frac{\partial \Omega^n}{\partial \omega_q^n} \tag{44}$$

and

$$\frac{\partial F}{\partial Q}\Omega^n = \sum_q^L \omega_q^n \frac{\partial F}{\partial Q}\frac{\partial \Omega^n}{\partial \omega_q^n} \tag{45}$$

Let

$$A_\ell^m = \iint \left[\frac{\partial}{\partial \xi}\left(\frac{\partial E}{\partial Q}\frac{\partial \Omega^m}{\partial \omega_\ell^m}\right) + \frac{\partial}{\partial \eta}\left(\frac{\partial F}{\partial Q}\frac{\partial \Omega^m}{\partial \omega_\ell^m}\right)\right] dS \tag{46}$$

Note that A_ℓ^m is not a function of ω's. Then, Eq. (43) becomes

$$\sum_i^I \sum_j^J (r^t)^* A_\ell^m = \sum_i^I \sum_j^J \sum_n^M \sum_q^L \omega_q^n (A_q^n)^* A_\ell^m \tag{47}$$

Let

$$C_{q\ell}^{nm} = \sum_i^I \sum_j^J (A_q^n)^* A_\ell^m \tag{48}$$

and

$$B_\ell^m = \sum_i^I \sum_j^J (r^t)^* A_\ell^m \tag{49}$$

Then

$$\sum_n^M \sum_q^L \omega_q^n C_{q\ell}^{nm} = B_\ell^m \tag{50}$$

or

$$\sum_n^M (\omega_1^n C_{1\ell}^{nm} + \omega_2^n C_{2\ell}^{nm} + \omega_3^n C_{3\ell}^{nm} + \ldots\ldots + \omega_L^n C_{L\ell}^{nm}) = B_\ell^m \tag{51}$$

resulting in a system of LxM equations for the unknown distributed optimal acceleration factors ω_ℓ^m. In the case of two-dimesional Euler equations, L = 4. Thus, we must solve the following system of 4xM equations in order to determine the 4xM optimal values of ω_ℓ^m.

$$\left[\begin{array}{cccc|ccc} C_{11}^{11} & C_{21}^{11} & C_{31}^{11} & C_{41}^{11} & C_{11}^{21} & \cdots & C_{41}^{M1} \\ C_{12}^{11} & C_{22}^{11} & C_{32}^{11} & C_{42}^{11} & C_{12}^{21} & \cdots & C_{42}^{M1} \\ C_{13}^{11} & C_{23}^{11} & C_{33}^{11} & C_{43}^{11} & C_{13}^{21} & \cdots & C_{43}^{M1} \\ C_{14}^{11} & C_{24}^{11} & C_{34}^{11} & C_{44}^{11} & C_{14}^{21} & \cdots & C_{44}^{M1} \\ \hline C_{11}^{21} & C_{21}^{21} & C_{31}^{21} & C_{41}^{21} & C_{11}^{21} & \cdots & C_{41}^{M1} \\ \vdots & \vdots & \vdots & \vdots & \vdots & \vdots & \vdots \\ C_{14}^{1M} & C_{24}^{1M} & C_{34}^{1M} & C_{44}^{1M} & C_{14}^{2M} & \cdots & C_{44}^{M4} \end{array}\right] \cdot \left[\begin{array}{c} \omega_1^1 \\ \omega_2^1 \\ \omega_3^1 \\ \omega_4^1 \\ \hline \omega_1^2 \\ \vdots \\ \omega_4^M \end{array}\right] = \left[\begin{array}{c} B_1^1 \\ B_2^1 \\ B_3^1 \\ B_4^1 \\ \hline B_1^2 \\ \vdots \\ B_4^M \end{array}\right] \qquad (52)$$

We have decided to use M = 4, that is, four consecutive global time steps.

Thus, four sequences of four optimal values of ω were used in Eq. 36 and Eq. 37 to update the solution to the next global time level.

RESULTS

The PBD and DMR concepts were applied to three model test cases: external flow around a cylinder, internal channel flow past a 10% circular arc, and external flow around a NACA 0012 airfoil.

Figure 1 shows the 65x33 O-type computational grid around a cylinder. Figures 2 and 3 show the convergence histories using the existing Artificial Dissipation (AD) model and the Physically Based Dissipation (PBD) model with and without the application of DMR with $M_\infty = 0.2$. Using DMR, the number of iterations needed to achieve the same level of residual is reduced by almost 50%. The savings in computational time is about 50% (Figures 4 and 5) using the AD and the PBD model with the application of DMR at $M_\infty = 0.2$. The savings in cpu time can be seen in Table 1, which presents the run times and residuals for several of the test cases. In Table 1, Res0 is the starting residual and Res is the final residual.

Figures 6 and 7 show convergence histories using the AD and the PBD with and without the DMR model for the $M_\infty = 0.4$. This is a clear indication that the present formulation of DMR is incapable of CPU time savings as the locally sonic flow conditions are approached.

At $M_\infty = 0.1$ the compressible Euler equations become a stiff system of partial differential equations. Figure 8 shows convergence history using the AD model with and without DMR. The large CPU time savings demonstrate the ability of DMR to treat stiff systems of equations (Figure 9).

Figure 10 illustrates the 65x17 H-type channel grid with a 10% circular arc bump on the floor. Figures 11-12 show that at $M_\infty = 0.5$ using the AD or the PBD model with the DMR yields about 50% savings in CPU time. Figures 13 and 14 show that using AD or the PBD model with DMR at $M_\infty = 0.6$ saves less than 50% in CPU time. The pressure contours using the AD and the PBD models were identical at $M_\infty = 0.6$ (Figure 15).

Figure 16 shows the 65x33 C-type clustered grid around a NACA 0012 airfoil. From Figure 17 it appears that using the AD model and DMR at $M_\infty = 0.63$ does not accelerate convergence. From Figure 18, the it is clear that using the PBD model allows the DMR to perform better even for this transonic shocked flow case resulting in over 30% saving in the CPU.

Finally, the PBD model was compared to the AD model by applying them to lifting and nonlifting transonic flows. The 129x33 C-type grid around a NACA 0012 airfoil is shown in Figure 19. Figure 20 shows isobars using the AD model at $M_\infty = 0.8$, $\alpha = 0.0°$. Figure 21 shows isobars when using the PBD model at $M_\infty = 0.8$, $\alpha = 1.25°$. Again, the PBD model yields a sharp shock.

CONCLUSIONS

A new physically based dissipation model has been presented. Advantages of the new model include:

1. The second order dissipation used in the PBD model represents actual physically consistent dissipation from the Navier-Stokes equations for compressible, viscous, heat conducting fluid flow.

2. The PBD model does not contaminate the continuity equation.

3. The PBD formulation maintains high accuracy. Actually, for flows with stronger shocks, the PBD formulation gives results comparable to TVD schemes.

4. The PBD concept can be applied to Navier-Stokes equations, too. The higher order physically consistent dissipation terms can be based on dissipation due to radiation heat transfer and heat generation due to chemical reactions.

5. An Euler solver with the PBD formulation easily converts to a Navier-Stokes solver by fixing the value of viscosity coefficient and by specifying no-slip boundary conditions on solid surfaces.

A conceptually new method termed Distributed Minimal Residual (DMR) has been developed and successfully applied to the acceleration of an explicit iterative algorithm for the numerical solution of a nonlinear system of Euler equations governing inviscid gasdynamics. The main idea of using a separate sequence of optimal acceleration factors for each of the equations in the system was theoretically formulated a numerically proven on a number of test cases. This means that the partial differential equations governing mass, x-momentum, y-momentum and energy conservation were accelerated according to their own separate optimal sequences of acceleration factors that have a common objective of minimizing the global residual of the entire system at each consecutive integration time step. DMR in its present form works best for low Mach number flows when the Euler equations become exceedingly stiff.

ACKNOWLEDGEMENTS

This work was supported by the Air Force Office of Scientific Research/Numerical Mathematics Program under the supervision of Dr. John P. Thomas and Dr. Arje Nachman. The manuscript was typed by Ms. Amy Myers.

REFERENCES

1. Jameson, A., Schmidt, W. and Turkel, E., "Numerical Solutions of the Euler Equations by Finite Volume Methods Using Runge-Kutta Time-Stepping Schemes," AIAA Paper No. 81-1259, Palo Alto, CA, June, 1981.

2. Pulliam, T. H., "Artificial Dissipation Models for the Euler Equations," AIAA Journal, Vol. 24, No. 12, December 1986, pp. 1931-1940.

3. Chima, R.V., Turkel, E., and Schaffer, S., "Comparison of Three Explicit Multigrid Methods for the Euler and Navier-Stokes Equations," NASA TM 88878, 1986; also ICOMP-86-3.

4. Caughey, D. A. and Turkel, E., "Effects of Numerical Dissipation on Finite-Volume Solutions of Compressible Flow Problems," AIAA paper 88-0621, Reno, NV, January 1988.

5. MacCormack, R. W. and Baldwin, B. S., "A Numerical Method for Solving the Navier-Stokes Equations With Application to Shock-Boundary Layer Interaction," AIAA paper 75-1, January 1975.

6. Salas, M. D., "Recent Developments in Transonic Euler Flow Over a Circular Cylinder," presented at the 10th IMACS World Congress on Systems Simulation and Scientific Computation, Montreal, Canada, August 8-13, 1982.

7. Abdy, G. L., "Inviscid Separation at Transonic Speeds," M.Sc. Thesis, Dept. of Mechanical and Aerospace Eng., Arizona State Univ., Tempe, AZ, December 1986.

8. Atkins, H. L., "Numerical Comparison of Time-Accurate Algorithms for a Nonlinear Shock-Propagation Problem," AIAA paper 85-1663.

9. Pandolfi, M. and Larocca, F., "Transonic Flow About a Circular Cylinder," proceedings of the conference in celebration of 60th birthday of Prof. G. Moretti, Aug. 1987.

10. Hughes, T., "Calculations of 2-D Euler Flows With a New Petrov-Galerkin Finite Element Method," Notes on Num. Fluid Mechanics, Vieweg-Verlag.

11. Raj, P. and Brennan, J., "Improvements to an Euler Aerodynamics Method for Transonic Flow Analysis," AIAA paper 87-0040, January 1987.

12. Chima, R. V., "Analysis of Inviscid and Viscous Flows in Cascades with an Explicit Multiple-Grid Algorithm," NASA TM 83636, 1983.

13. Jameson, A. and Mavriplis, D., "Finite Volume Solution of the Two-Dimensional Euler Equations on a Regular Triangular Mesh," AIAA Journal, Vol. 24, No. 4, April 1986, pp. 611-618.

14. Dulikravich, G. S., Dorney D. J., and Lee, S. S., "A Physically Based Dissipation (PBD) Model for the Euler Equations of Gasdynamics," submitted for publication.

15. Wambecq, A., "Rational Runge-Kutta Methods for Solving Systems of Ordinary Differential Equations," Computing, Vol. 20, 1978, pp. 333-342.

16. Hafez, M., Parlette, E., and Salas, M. D., "Convergence Acceleration of Iterative Solutions of Euler Equations for Transonic Flow Computations," AIAA Paper 85-1641, July 1985.

17. Kennon, S. R., and Dulikravich, G. S., "Optimal Acceleration Factors for Iterative Solution of Linear and Nonlinear Differential Systems," Computer Methods in Applied Mechanics and Engineering, 47, 1984, pp. 357-367.

18. Kennon, S. R., "Optimal Acceleration Factors for Iterative Solution of Linear and Nonlinear Differential Systems," AIAA Paper 85-0162, January 1985, Reno, Nevada.

19. Huang, C. Y., Kennon, S. R., and Dulikravich, G. S., "Generalized Nonlinear Minimal Residual (GNLMR) Method for Iterative Algorithms," Journal of Computational and Applied Mathematics, 16, 1986, pp. 215-232.

20. Huang, C. Y. and Dulikravich, G. S., "Fast Iterative Algorithms Based on Optimized Explicit Time-Stepping," Computer Methods in Applied Mechanics and Engineering, 63, August 1987, pp. 15-36.

21. Dulikravich, G. S., Mortara, K. W. and Marraffa, L., "A Physically Consistent Model for Artificial Dissipation in Transonic Potential Flow Computations," AIAA paper 88-3654 presented at the 1st National Congress of Fluid Dynamics, Cincinnati, OH, July 1988.

ARTIFICIAL DISSIPATION METHOD

Cylinder

M	No DNLMR	DNLMR	Res	Res0
0.1	1778.12	735.63	-3.0	-0.7441330
0.2	1774.30	837.39	-2.8	-0.4233154
0.3	2094.92	1251.21	-3.7	-0.2269995
0.4	2063.57	1835.53	-4.5	-8.1262559E-02

Airfoil

M	No DNLMR	DNLMR	Res	Res0
0.63	1499.51	1735.21	-2.9	1.009068

PHYSICALLY BASED DISSIPATION METHOD

Cylinder

M	No DNLMR	DNLMR	Res	Res0
0.2	2212.95	1594.33	-2.4	-0.4341858
0.3	1986.46	1548.81	-2.7	-0.2433041
0.4	2442.75	2164.490	-3.0	-0.1030241

Airfoil

M	No DNLMR	DNLMR	Res	Res0
0.63	2612.46	1529.06	-0.78	0.9581382

Table 1.

Comparison of CPU time (sec) for Artificial Dissipation (AD) and Physically Based Dissipation (PBD)

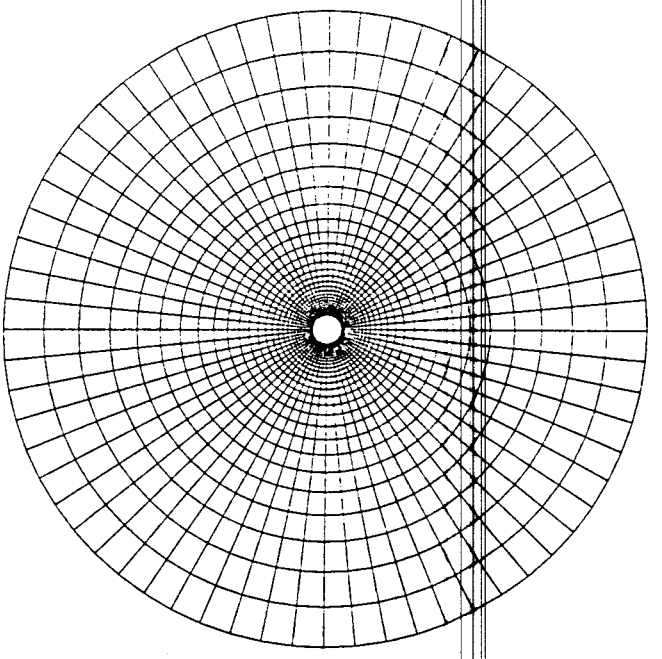

Figure 1.

Circle: Computational O-type grid (65 x 33)

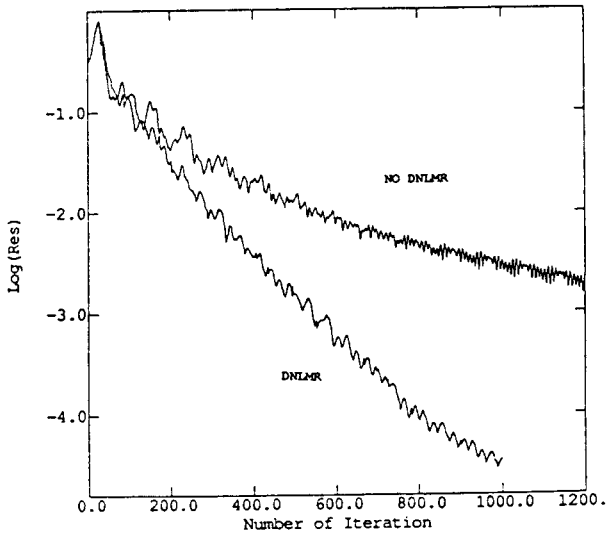

Figure 2.

Circle: Convergence history; AD; M_∞= 0.2.

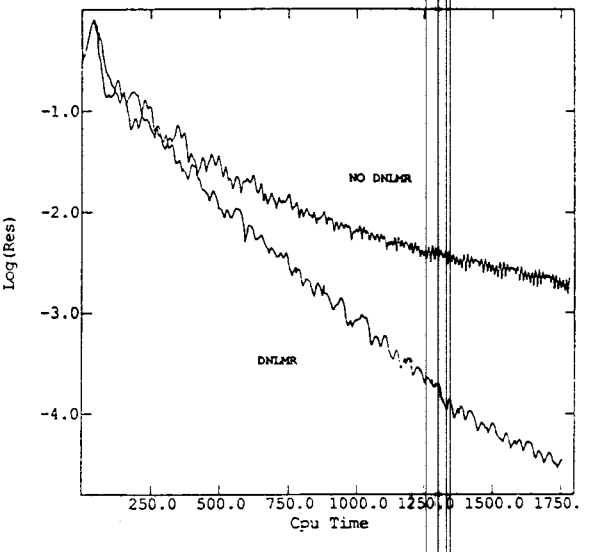

Figure 3.

Circle: Convergence history; PBD; M_∞= 0.2.

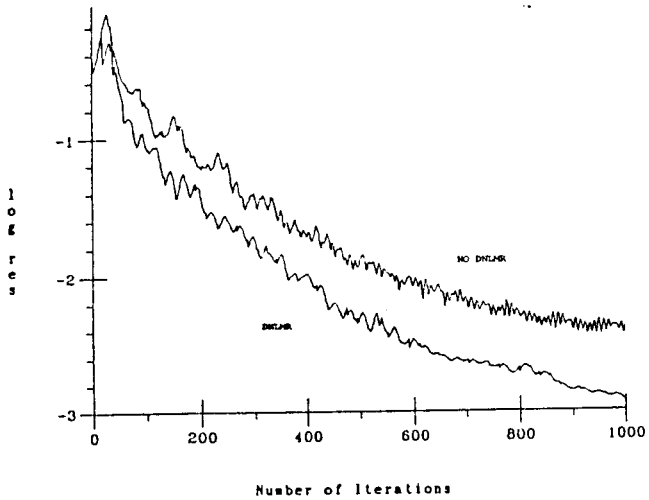

Figure 4.

Circle: CPU history; AD; M_∞= 0.2.

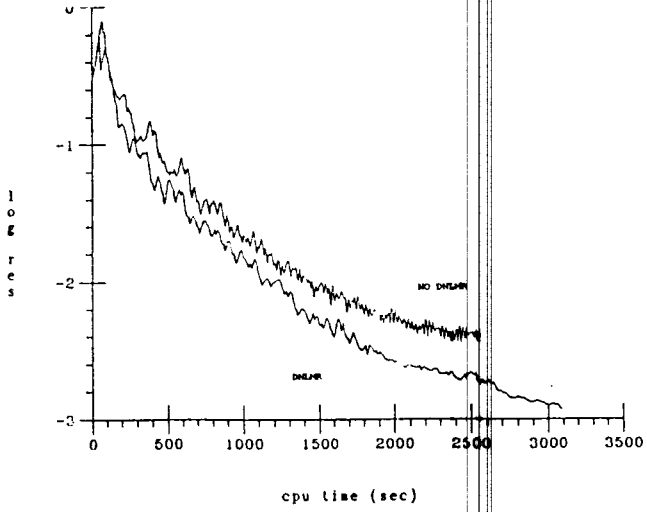

Figure 5.

Circle: CPU history; PBD; M_∞= 0.2.

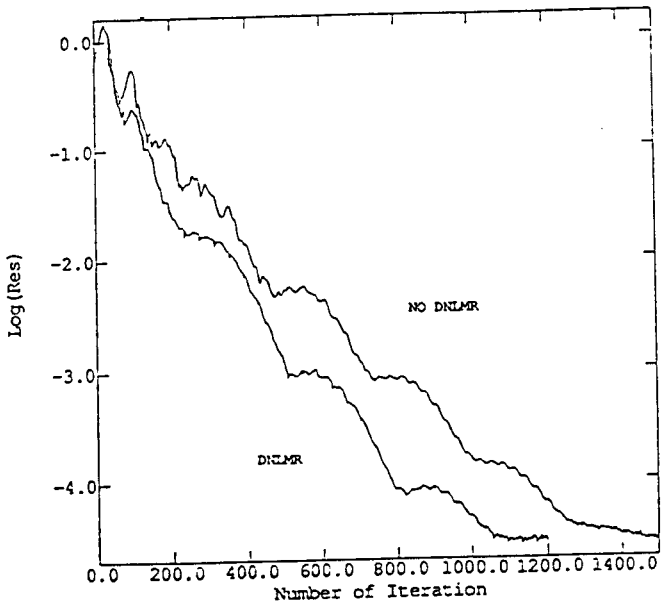

Figure 6.

Circle: Convergence history; AD; M_∞= 0.4.

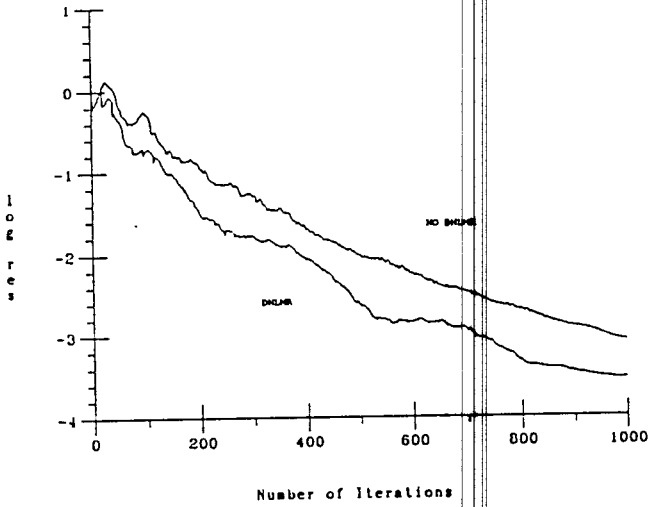

Figure 7.

Circle: Convergence history; PBD; M_∞= 0.4.

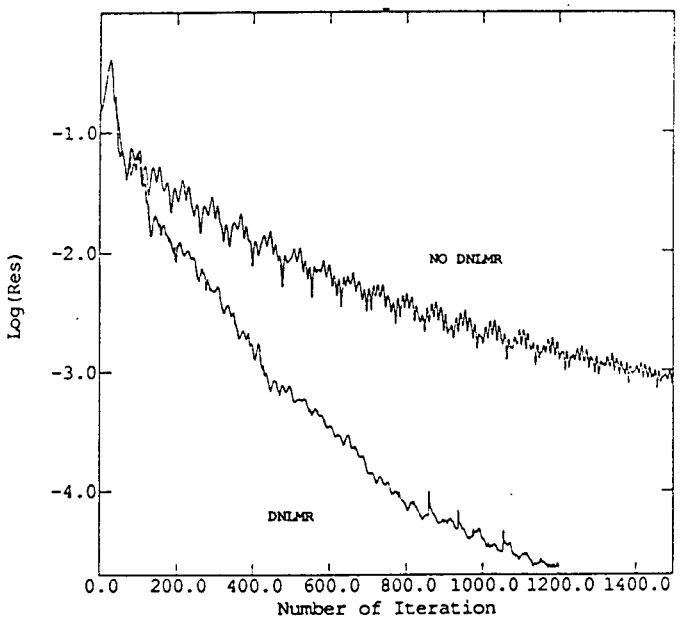

Figure 8.

Circle: Convergence history; AD; M_∞= 0.1.

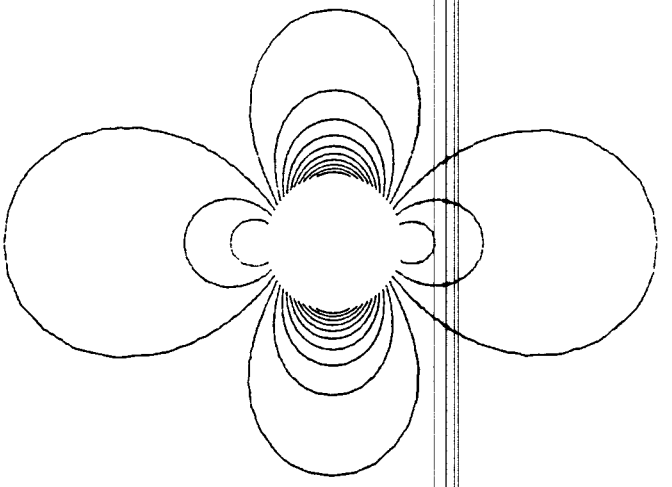

Figure 9.

Circle: Isobars; AD; M_∞= 0.1.

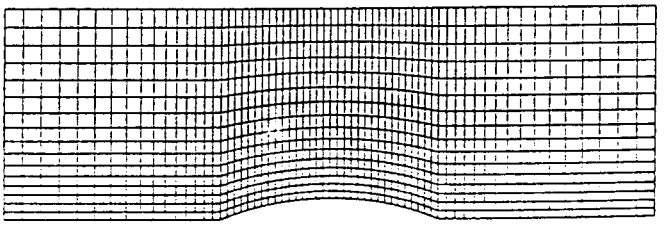

Figure 10.

Channel: Computational grid (65 x 17)

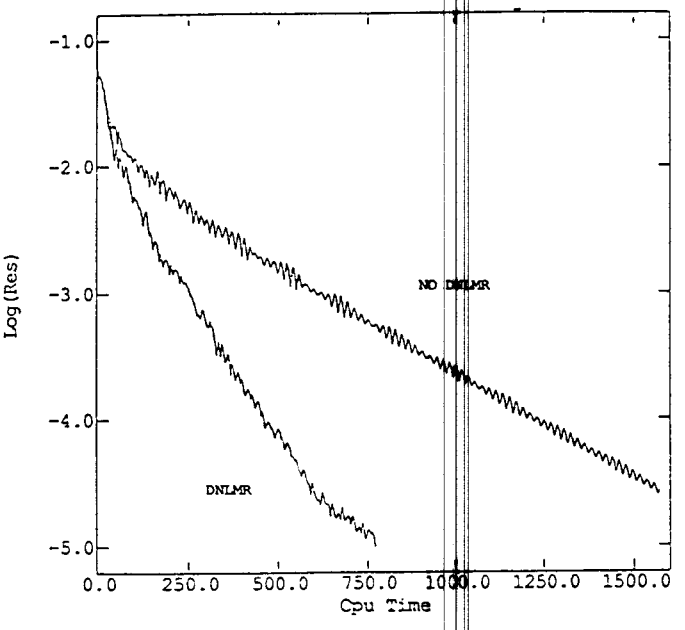

Figure 11.

Channel: CPU history; AD; M_∞= 0.5.

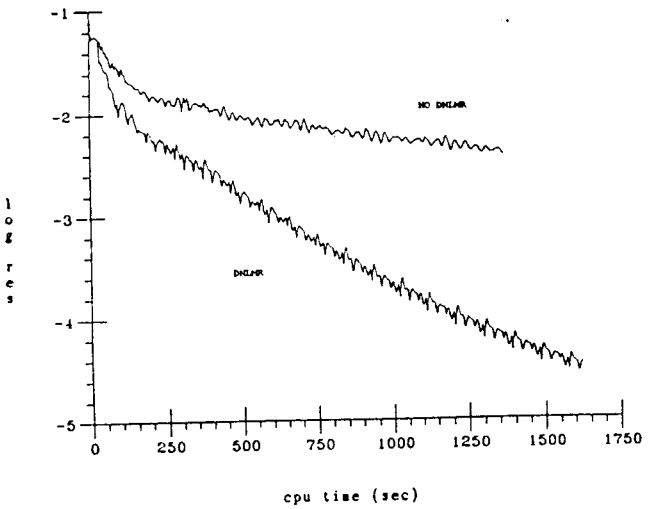

Figure 12.

Channel: CPU history; PBD; M_∞= 0.5.

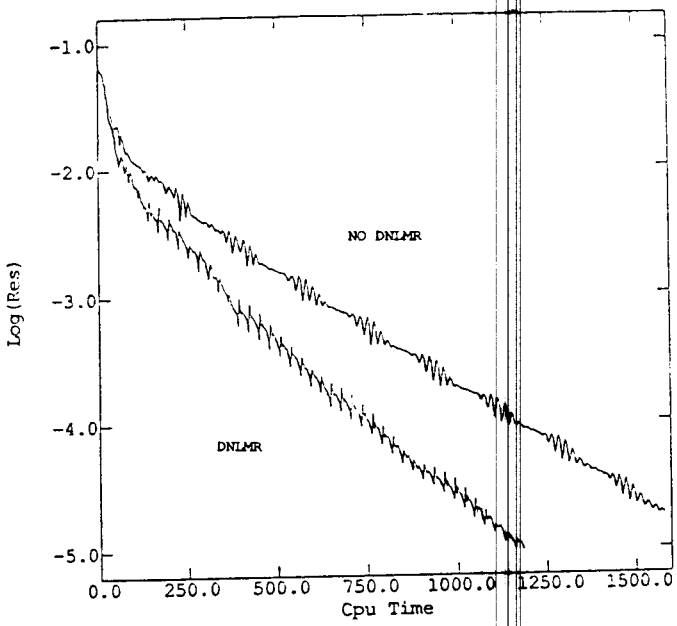

Figure 13.

Channel: CPU history; AD; M_∞= 0.6.

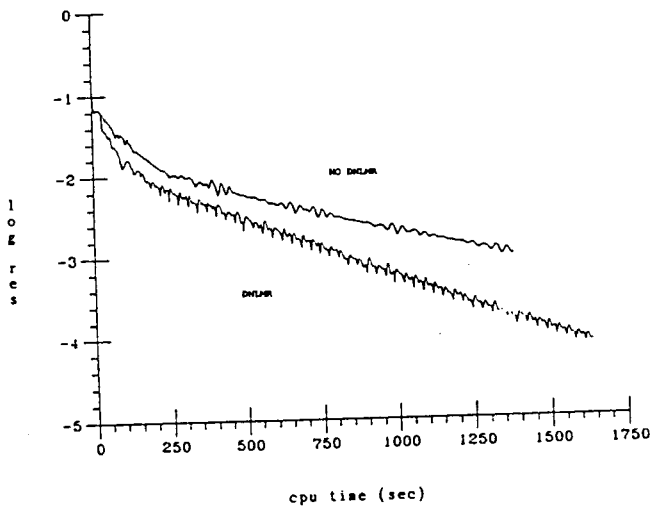

Figure 14.

Channel: CPU history; PBD; M_∞= 0.6.

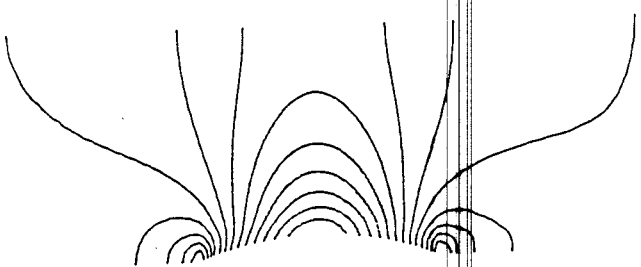

Figure 15.

Channel: Isobars; AD & PBD; M_∞= 0.6.

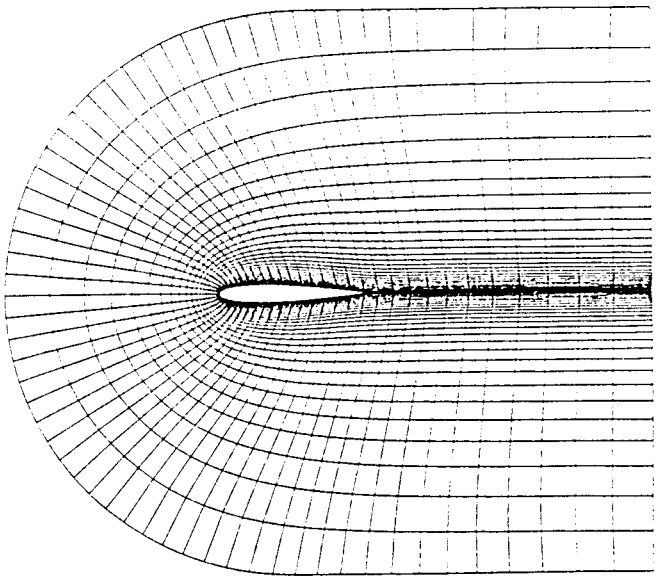

Figure 16.

NACA0012: Computational grid (65 x 33)

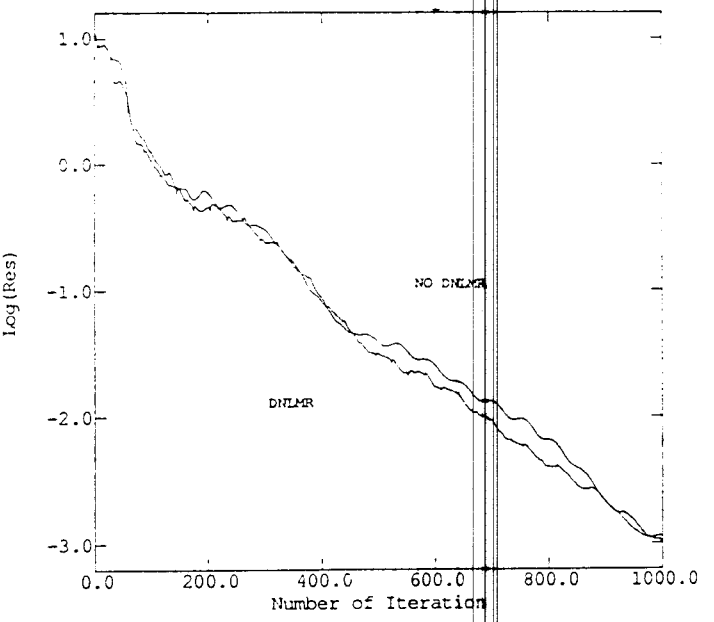

Figure 17.

NACA0012: Convergence history; AD; M_∞= 0.63.

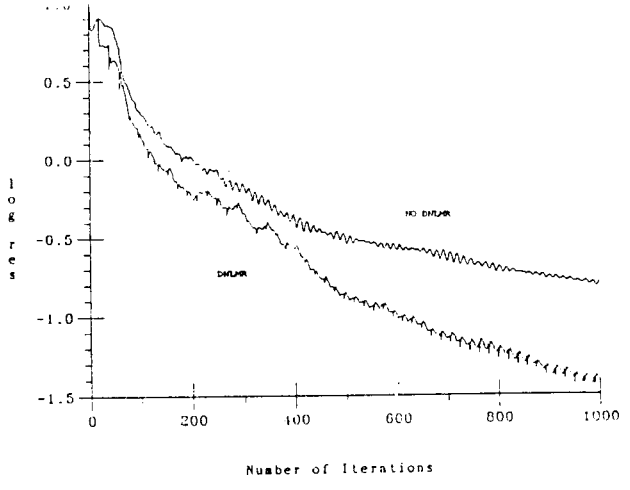

Figure 18.

NACA0012: Convergence history; PBD; M_∞= 0.63.

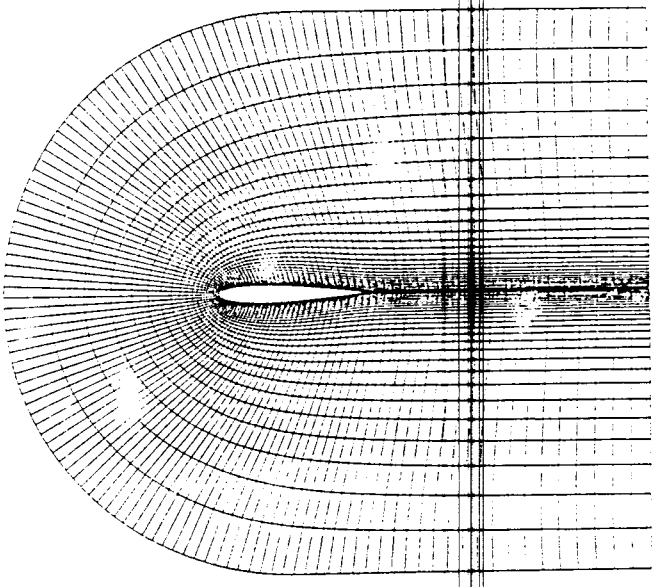

Figure 19.

NACA0012: Computational grid (129 x 33)

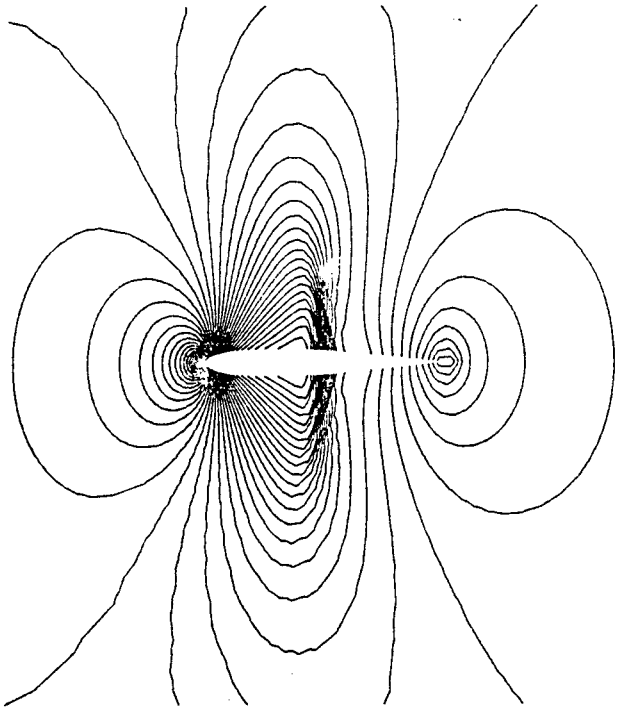

Figure 20.

NACA0012: Isobars; AD; $M_\infty = 0.8; \alpha = 0.0°$.

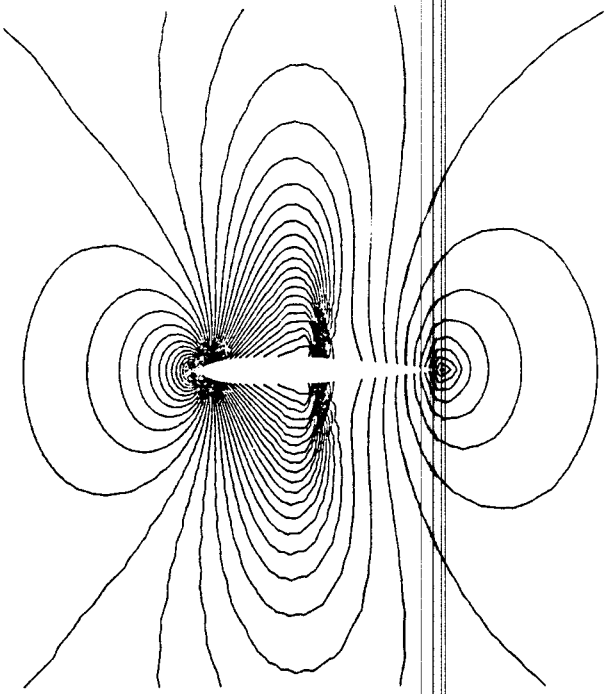

Figure 21.

NACA0012: Isobars; PBD; $M_\infty = 0.8; \alpha = 0.0°$.

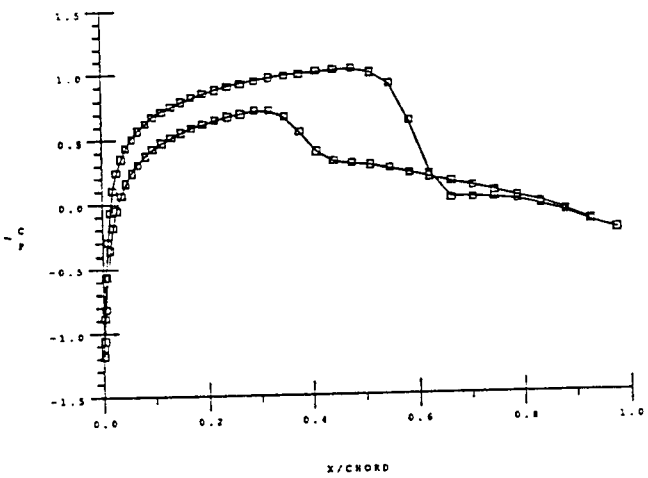

Figure 22.

NACA0012: Surface pressure coefficients; AD; $M_\infty = 0.8; \alpha = 1.25°$.

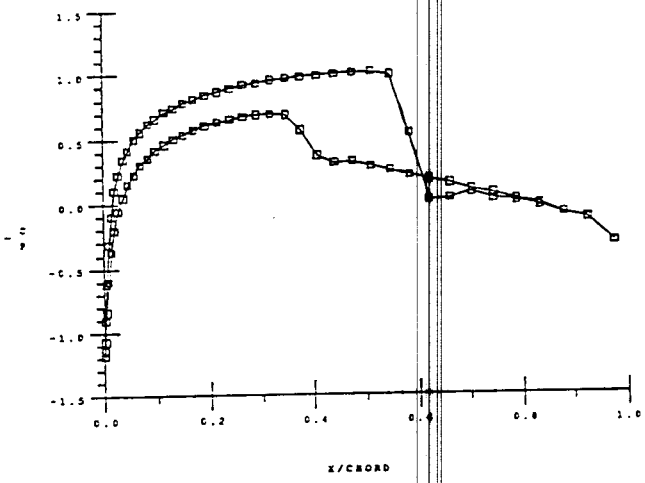

Figure 23.

NACA0012: Surface pressure coefficients; PBD; $M_\infty = 0.8; \alpha = 1.25°$.